Near-infrared high-*Q* all-dielectric metasurface biosensor based on quasi-bound state in continuum*

WANG Junhui[1], LI Deqiong[2], NIE Guozheng[1, 3, *], ZHAN Jie[1], GAN Longfei[3], CHEN Zhiquan[3], LAN Linfeng[4, *]

1. Hunan Provincial Key Laboratory of Intelligent Sensors and New Sensor Materials, School of Physics and Electronic Science, Hunan University of Science and Technology, Xiangtan 411201, China
2. School of Mathematics and Statistics, Hunan University of Technology and Business, Changsha 410205, China
3. School of Microelectronics and Physics, Hunan University of Technology and Business, Changsha 410205, China
4. Luminescence Materials and Devices National Key Laboratory, South China University of Technology, Guangzhou 510640, China

Abstract

In recent years, Bound States in the Continuum (BICs) have become a hot research topic because of their strong ability to facilitate light-matter interactions, and they are also an ideal platform for realizing optical resonances with ultra-high quality factors (*Q*). Nowadays, BICs have been found to exist in various photonic microstructures and nanostructures such as waveguides, gratings, and metasurfaces, among which metasurfaces have attracted much attention due to their ease of adjustment and considerable robustness. Traditional precious metal-based metasurfaces inevitably have low *Q*-factors due to the inherent defect of high ohmic losses. In contrast, due to lower ohmic losses, all-dielectric metasurfaces can be an excellent alternative to metallic metasurface structures. In this work, an all-dielectric metasurface is designed, with a silicon disc as the unit cell, and symmetric protected BIC (SP-BIC) is observed on the metasurface. When introducing eccentric holes to break the symmetry in the structural

* The paper is an English translated version of the original Chinese paper published in Acta Physica Sinica. Please cite the paper as: WANG Junhui, LI Deqiong, NIE Guozheng, ZHAN Jie, GAN Longfei, CHEN Zhiquan, LAN Linfeng，**Near-infrared high-*Q* all-dielectric metasurface biosensor based on quasi-bound state in continuum** . *Acta Phys. Sin.*, 2025, 74(10): 107801. doi: 10.7498/aps.74.20241752

plane (QBIC), the SP-BIC can be transformed into a quasi-BIC, with radiation dominated by magnetic dipoles and has a high-quality *Q*-factor. For QBICs formed on the metasurface, the resonance wavelength is usually greatly dependent on the refractive index of the surroundings due to the strong localization of the electric field within the cell. As the refractive index of the background changes, the positions of the resonance peaks change accordingly, and identification sensing of some biological components is achieved by this principle. This metasurface-based bio-refractive index sensor is less invasive in free space and is expected to overcome the drawbacks of traditional electrochemical-based biosensing technologies, which have cumbersome detection steps and high time and material costs. In terms of sensing parameters, due to the quadratic inverse relationship between the quality factor and asymmetric parameters, by adjusting the asymmetric parameters, the quality factor will also change, thereby enhancing and adjusting the sensing performance. After adjusting, the refractive index sensing sensitivity and figure of merit of this metasurface reach 162.55 nm/RIU and 1711.05 RIU^{-1}, respectively, which are higher than those achieved in many other existing studies. This high *Q*-factor all-dielectric metasurface design provides a new avenue for achieving high-sensitivity and high-precision bio-detection.

Keywords: all-dielectric metasurface; bound states in the continuum; refractive index sensing; optical biosensing
PACS: 78.67.-n; 07.07.Df; 87.85.fk; 42.60.Da
doi: 10.7498/aps.74.20241752
cstr: 32037.14.aps.74.20241752

1. Introduction

Waves that are completely confined in the continuum of radiating waves without interacting with them are called bound states in the continuum (BICs), which are unique fully confined modes[1,2]. Because of its strong enhancement of the local electric field at the nanoscale, it has attracted wide attention in the modern nanophotonics community[3]. The concept of BIC originated from quantum mechanics and was proposed by von Neumann and Wigner in 1929 based on the Schrodinger equation[4]. Since then, it has been extensively studied in different areas of wave physics, including acoustics, microwaves, water waves, and nanophotonics[5–15]. In 2008, the concept of BIC was first introduced into the field of optics[16]. Since then, various optical structures, such as nano-photonic crystal sheets, optical waveguide arrays, and superstructured surfaces, have successively achieved high quality factor (*Q*) resonance through BICs[17–19]. In recent years, nanophotonic structures have become a particularly attractive platform because of

the ability to customize materials and structures. The ideal BIC is completely decoupled from the free space radiation, so it has a theoretically infinite quality factor, and the radiation lifetime tends to be infinite[20], which shows that the resonance linewidth of Fano resonance disappears and the energy is localized in the nanostructure. BIC can be divided into two types according to the physical mechanism of decoupling: one is the accidental BIC[9,21] caused by the continuous adjustment of system parameters; the other is the (symmetry-protected BIC SP-BIC) caused by the breaking of spatial symmetry, which leads to the decoupling of discrete modes and continuous radiation modes[22]. In a photonic crystal slab, the mode above the ray of the band structure is usually radiative due to coupling with the continuum of extended modes. However, due to the symmetry mismatch between their mode profile and the external propagating mode, some bound States can exist even above the ray of the band structure. At the Γ point of the photonic crystal band, when the operating frequency is below the diffraction limit, the only radiation state is the normal plane wave[23], whose electromagnetic field distribution is odd under 180 ° rotation around the *z* axis, that is C_2 symmetry, so any even mode at the Γ point is BIC[24], because the overlap between their mode distribution and the outgoing wave is zero. Because SP-BIC is common and easy to implement, it has been found in various photonic micro-nano structures, such as waveguide[25,26], grating[27,28] and metasurface[29]. A symmetry-protected BIC is an ideal BIC that does not radiate energy outward and has zero linewidth, so it cannot be detected in the spectrum. In practical applications, asymmetric factors (such as eccentric hole, split, inhomogeneous refractive index, highly tilted, etc.) Are usually introduced into the system to break the symmetry of the structure, resulting in the coupling between the SP-BIC and the continuum radiation, establishing a radiation channel and transforming the SP-BIC into a quasi-bound state (QBIC). QBIC can be considered as a leaky mode with a finite but huge *Q* factor occurring near the BIC, which can greatly enhance the local field and the light-matter interaction, and shows a sharp Fano profile in the transmission spectrum. At the same time, it can be directly excited by an external light source without a special coupling mechanism. Currently, the QBIC mechanism has been used in various applications, such as filter[3], laser[30], nonlinear device[24], and sensor[31].

In the past decade, metasurfaces have attracted much attention due to their tunability and robustness. It has been demonstrated that the drastic change of the Q factor can be achieved by adjusting the asymmetry of the photonic crystal structure unit[32]. Among them, traditional metasurfaces based on noble metals inevitably have low Q factors due to the inherent defect of high ohmic loss[33,34]. All-dielectric metasurfaces are expected to be excellent alternatives to plasmonic metasurfaces due to their flexible tunability, low ohmic loss, strong locality, and ultra-compact structure. Up to now, many metasurface structures supporting QBIC high Q resonances have been proposed, such

as tilted dielectric ridge[35], dielectric split ring[36], and dielectric cubes of unequal size[37]. In practical applications, optical sensing based on the spectral shape of the optical resonance caused by the change of the medium environment, the change of the resonance wavelength and intensity has been successfully demonstrated[19,38]. For QBIC formed on metasurfaces, due to the strong localization of the electric field within the unit cell, the resonance wavelength usually has a strong dependence on the refractive index of the surrounding environment[39], which is usually used to realize optical sensing. The high*Q* factor of QBIC can bring high sensitivity and greater figure of merit to optical sensors.

In the past few decades, the application of optics in biosensing has attracted great attention in the fields of biochemistry and medicine[40–42]. Especially in cell scanning imaging and biological protein detection and identification. However, the traditional electrochemical-based biosensing technology is usually cumbersome in terms of equipment and detection steps. For example, when using transmission electron microscopy to observe and analyze cells and biological proteins, the cost of time and materials is very high, and the sample preparation process is complex, which limits its application[43,44] in basic research. The traditional biosensing method based on fluorescence labeling also has the disadvantages of requiring complex instruments and labels, not being able to detect in real time, causing certain damage to the sample, and being expensive. Relatively speaking, optical biosensing technology has low invasiveness to overcome the above shortcomings. In addition, because optical biosensors have relatively stable and non-conductive sensing elements, they also show strong advantages in complex environments, such as strong electric fields, strong electric waves or extreme temperature conditions[45,46]. In recent years, many new optical mechanisms for biosensing have been proposed, such as microcavity[47], surface plasmon[48] and micro-nano suspended channel resonator[49]. Although these new methods have shown potential for practical applications in some areas, they still have some inherent drawbacks, such as high resistance losses, complex structural design, and low tunability. As a unique new mechanism for enhancing light-matter interaction, all-dielectric metasurfaces supporting QBIC have not been fully exploited in the field of biosensing. At present, the research on BIC sensors mainly focuses on the basic sensing of refractive index and temperature change[50,51], and the research on biosensing is less, and the sensing parameters are relatively low. Therefore, it is necessary to propose a new label-free, rapid and real-time method for the efficient detection of biological proteins with higher sensitivity and lower cost.

In this paper, we propose a possible method for detecting biological proteins on all-dielectric metasurfaces supporting high-quality magnetic dipole (MD) QBIC

resonances with Q factors higher than 10^5. Breaking the in-plane structural symmetry by introducing an eccentric hole, the SP-BIC transforms into a QBIC with an ultrahigh Q factor, accompanied by a huge local field enhancement. At the same time, it has lower ohmic loss and higher tunability than the traditional plasmonic metasurface. By controlling the value of the asymmetry parameter, the spectral line width of the QBIC mode can be flexibly controlled, and the quality factor can be theoretically improved to an arbitrary value, so that the sensing performance can be improved and adjusted. By adjusting, the figure of merit (FOM) can be as high as 1711.05 RIU^{-1}, which is higher than many reported results based on other traditional methods. The sensing performance of high FOM endows the sensor with higher accuracy in the detection of biological proteins, which can detect small refractive index changes more accurately, thus providing more reliable detection results. It can be seen that the biosensor based on QBIC has excellent performance. In addition, the simple design allows the sensor to adapt to a variety of complex detection environments, which further expands its application prospects in the field of biomedical detection. The results of this study demonstrate the potential of this new sensor. This all-dielectric metasurface design with high Q factor is expected to play an important role in the development of future biosensors, providing a new way for high-sensitivity and high-precision biological detection.

2. Structure design and simulation

The minimum structural unit of the designed all-dielectric metasurface structure is shown in Fig. 1. A silicon nanodisc with radius R = 300 nm and height H = 100 nm is placed on a glass substrate with thickness of 1000 nm. The periodic size of the structural unit is $P_x = P_y$ = 900 nm. An eccentric hole with a variable radius r is introduced within a fixed distance of 150 nm from the center of the nanodisc, as shown in Fig. 1(b). The in-plane symmetry is broken, which allows the establishment of radiation channels and the transition of the resonance state from the symmetry-protected BIC to the quasi-BIC. By changing the size of the radius r, the asymmetry of the structure can be regulated, and then the quasi-BIC resonance can be regulated. The simulation is carried out in the commercial software Lumerical FDTD Solutions, using the (finite-difference time-domain method, FDTD), which has been proved to be an effective means to provide accurate predictions for electromagnetic interaction problems[52]. The light source of the system is set as a near-infrared plane wave of 1400-1700 nm incident along the $-z$ axis, and the electric field and magnetic field are polarized along the y axis and x axis, respectively. Therefore, the periodic boundary condition is used in the x-y plane, and the perfect matched layer is used in the z direction. To simulate convenience, the refractive indices of

silicon and glass were set to 3.48 and 1.5, respectively, and the background was set to a uniform background with a refractive index of 1.

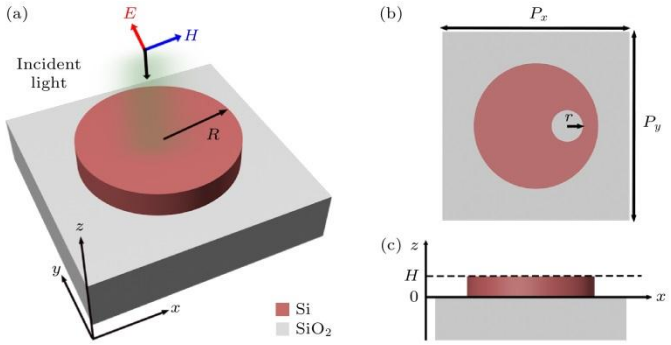

Figure 1. (a) Schematic of the proposed all-dielectric metasurface, the structural parameters are P_x = P_y = 900 nm, R = 300 nm, H = 100 nm, and the thickness of the glass substrate is set to 1000 nm; (b) an off-centered hole with variable radius r is introduced at a fixed distance of 150 nm from the center of the disc to break the C_2 symmetry of the structure; (c) front view of the silicon nanodisc metasurface.

As shown in Fig. 2(a), an ideal independent periodic array of silicon nanodisks with C_2 symmetry without a substrate is first considered. To find the BIC, a dipole cloud was used to excite all possible resonant modes supported by the periodic array[53], and the resulting photonic band structure is shown in the Fig. 2(b). The location of the SP-BIC is marked by a red circle in the figure, which is at the Γ point of the first Brillouin zone and within the frequency range of the second near-infrared region. Its corresponding frequency is below the diffraction limit of the given periodic structure, in which case the only radiation channel is a plane wave propagating in the normal direction[23]. The electromagnetic field vector of the SP-BIC mode is odd under the C_2 symmetry. Due to the symmetry mismatch, the resonant mode becomes completely confined and no longer couples with other radiation channels in free space, which leads to a theoretical infinite Q factor[22,54]. When the in-plane symmetry is broken by the introduction of defects, the radiation channel will be opened, so that the SP-BIC will be transformed into a QBIC with a finite and huge Q factor, which shows a clear Fano feature in the optical response spectrum.

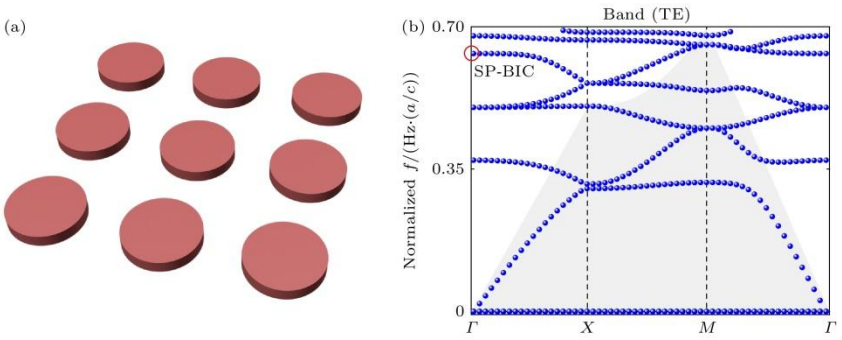

Figure 2. (a) Schematic of a metasurface consisting of periodically aligned arrays of silicon nanodiscs; (b) calculated photonic band structure of the periodically aligned silicon nanodisk array in panel (a), grey shading indicates the region located below the free-space light cone, the location of the trapped symmetrically protected BIC is marked with a red circle.

In practice, periodically arranged silicon nanodisks cannot be suspended in air, so a glass substrate with a low loss index is introduced here. The presence of the substrate will cause a small amount of bound energy to leak out of the open radiation channel in the substrate, resulting in a reduction in the Q factor[24]. However, the SP-BIC supported by the proposed structure is quite robust[55], and the presence of the substrate does not have a significant impact. QBIC resonance is closely related to radiation leakage, so the radiation rate and transmission line width can be adjusted by controlling the geometric parameters. With the increase of the eccentric hole radius, the linewidth of the transmission spectrum at the resonance of the QBIC increases gradually. In order to show the transition from SP-BIC to QBIC more intuitively, the transmission spectrum with the change of the eccentric hole radius is calculated as shown in the Fig. 3(a). It can be seen from the Fig. 3(a) that when the eccentric hole radius *r* is zero, the transmission linewidth is also zero, which means that the resonance peak disappears and no energy leaks from the bound state to the free-space continuum state, and the corresponding Q factor is theoretically infinite. When the *r* increases, the propagation dip is slightly blue-shifted and broadened, and the QBIC exchanges energy with the continuous free-space radiation mode, resulting in a sharp Fano resonance[32]. As shown in Fig. 3(b), considering the single case of r = 75 nm, it can be seen from Fig. 3(b) that the transmission spectrum shows an asymmetric line shape and a narrow dip at λ = 1458.11 nm, which is in good agreement with the Fano line shape in the framework of the classical (coupled-mode theory CMT). To illustrate this, the transmission spectrum is fitted by the classical Fano formula[56,57]:

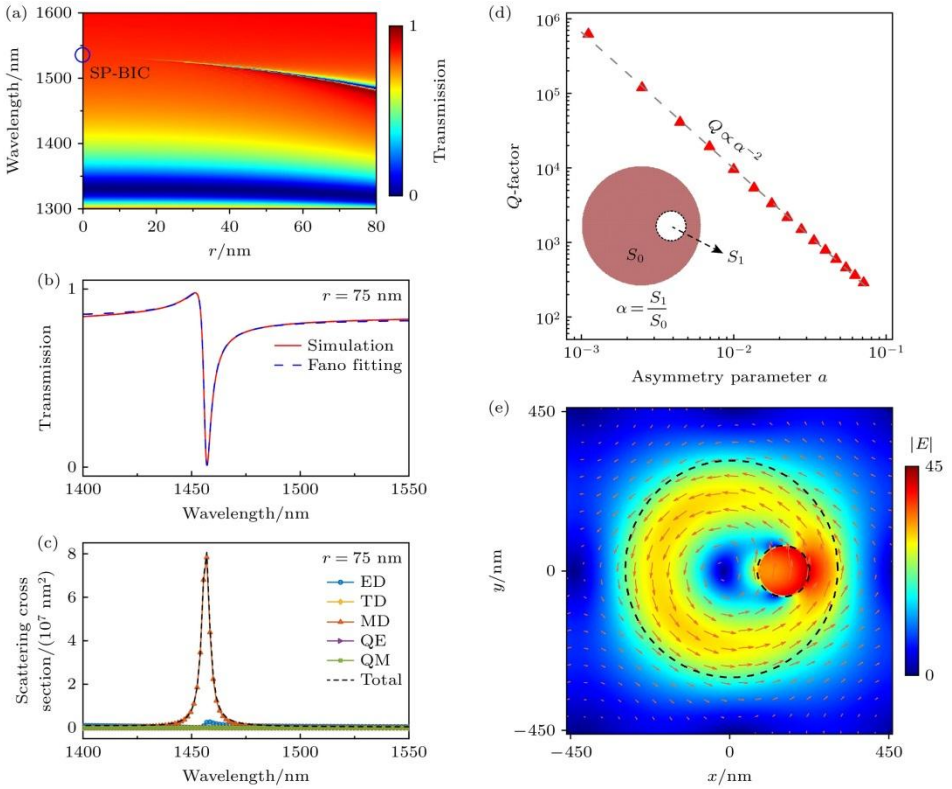

Figure 3. (a) Transmission spectrum of the silicon nanodisk metasurface on a glass substrate concerning the radius of the off-centered hole, the corresponding position of the SP-BIC is marked using a basket circle; (b) transmission spectrum a*t* r = 75 nm and comparison with the fitted curve of Fano's formula; (c) the multilevel unfolding of the silicon metasurface resonance at r = 75 nm shows that the MD response is dominant at the resonance wavelength position; (d) the relationship between the Q-factor and the asymmetry parameter α, which is plotted in logarithmic coordinates to visualize the relationship; (e) image of the x-y plane electric field distribution at resonance in the case of r = 75 nm, with the red arrows indicating the in-plane circulating displacement currents.

$$T(\omega) = T_0 + A_0 \frac{[q+2(\omega-\omega_0)/\gamma]^2}{1+[2(\omega-\omega_0)/\gamma]^2}, \qquad (1)$$

Where ω_0 is the resonance center frequency, γ is the resonance linewidth, T_0 is the background scattering parameter, A_0 is the coupling coefficient between the continuum state and the discrete state, and q is the Breit-Wigner-Fano parameter, which determines the asymmetry of the resonance curve. According to the fitting formula, we can calculate $Q = \omega_0/\gamma$ [58]. As shown in Fig. 3(d), the Q factor of the QBIC mode for different eccentric hole radii is calculated and plotted as a function of the asymmetry parameter, where the asymmetry parameter α is defined as the ratio of the eccentric hole area (S_1) to the original silicon disk area (S_0):

$$\alpha = \frac{S_1}{S_0} = \frac{r^2}{R^2}. \quad (2)$$

In order to see the relationship between the Q factor and the asymmetry parameter α more intuitively, the coordinates in the figure are plotted with $\log_{10}$-$\log_{10}$ scale. From the Fig. 3(d), it can be seen that the Q factor and α have an obvious inverse quadratic relationship[32] in the appropriate range:

$$Q(\alpha) = Q_0[\alpha]^{-2}, \quad (3)$$

Where Q_0 is a constant determined by the metasurface structure and is independent of the asymmetry parameter α. The results show that the Q factor of the QBIC resonance supported by the silicon nanodisk can be adjusted over three orders of magnitude with the change of the radius of the eccentric hole, which can actively adjust the coupling efficiency and the Q factor to a great extent, and such a large Q factor also provides a great application prospect for the realization of high-resolution optical biosensors. In order to further explore the radiation mechanism of QBIC resonance, as shown in Fig. 3(c), through the multi-level decomposition[59,60] of the scattering cross section of the optical resonance response at r = 75 nm, it is found that the radiation power of MD is the largest, and the contribution of other polar resonances is very weak, which further indicates that this QBIC radiation state is absolutely dominated by MD response, which represents the radiation channel coupled with the outgoing wave in the system. The near-field distribution of the electric field on the corresponding x-y plane when the Fig. 3(e) is r = 75 nm. From the Fig. 3(e), it can be seen that the electric field is greatly enhanced at the eccentric hole, indicating that the incident light along the $-z$ direction is strongly trapped in the metasurface by the magnetic dipole oscillation, and the huge Q factor can significantly enhance the interaction between local light and matter. The superimposed arrows indicate the in-plane circulating displacement current, which is typical of magnetic dipole resonance[61,62].

In the actual manufacturing process, high Q factor metasurfaces require high manufacturing process, because their near-field coupling effect is very sensitive to manufacturing errors, which will lead to more light radiation into free space and reduce the Q factor. Therefore, achieving a high Q factor requires a reduction in scattering losses due to manufacturing errors. Although this study is limited to the simulation level, some recent literature has provided further support for our experimental feasibility. In 2024, Hu et al. Demonstrated the actual fabrication of tunable cuboid array metasurface based on QBIC[63], and the experimental and simulation results were integrated. For the preparation of the proposed metasurface structure, a silicon film was first deposited on a SiO_2 substrate by (low-pressure physical vapor deposition LPCVD), and then ZEP520

resist was uniformly spin-coated on the sample and baked. Next, the desired metasurface can be obtained by (electron beam lithography EBL) and (inductively coupled plasma etching ICP). Finally, plasma cleaning is performed after the resist is removed. The desired metasurface can be fabricated with only a few simple processes.

3. Results and Discussion

The QBIC resonance mode supported by the proposed metasurface structure corresponds to a wavelength in the near-infrared two-region range, which is often used for biological and medical detection. In general, the resonant wavelength position of the metasurface structure also changes with the change of the surrounding dielectric constant, and with the increase of the effective refractive index, there will be a red shift in the transmission spectrum[64]. Therefore, the study in this paper also has the potential to be used as a biosensor. In this paper, the influence of different biological components (the refractive index of different biological components is denoted as RI) on the QBIC resonance is simulated by changing the refractive index of the background environment. Under the default condition, the background is ideal air, so the background refractive index (denoted as n_B) is set to $n_B = 1$. In the selection of the eccentric hole radius, although the smaller the radius r, the larger the Q factor obtained, the narrower the resonance linewidth, and the larger the corresponding figure of merit. However, considering that the amplitude signal of the formant will decrease with the decrease of the radius r, the formant will disappear completely when $r = 0$, which is not conducive to the detection of the detection instrument in practical application. After comparative screening, the radius of the eccentric hole here is $r = 25$ nm. According to the Q-α relationship in Fig. 3(d), the Q factor at this time can reach an astonishing level of 10^5. As shown in the Fig. 4(a), the transmission spectrum has an obvious red shift with the increase of the background refractive index, because the increase of the background refractive index will lead to the decrease of the overall effective refractive index of the metasurface structure unit. Here, the background refractive index n_B varies from 1.00 to 1.48, and the refractive index of many biological components is in this range, such as saline (NS, RI = 1.33), white blood cells (WBC, RI = 1.36), red blood cells (RBC, Ri = 1.40), and protein, RNA or DNA (Ri = 1.46) [65–67]. In order to further study this performance, the relationship between the resonance peak wavelength position (λ_{dip}) and the full width at half maximum (FWHM) of the transmission spectrum and n_B is analyzed, and the results are shown as Fig. 4(b),(c). From the Fig. 4, it can be seen that there is a linear relationship between the λ_{dip} and FWHM and the background refractive index n_B , which can be used to sense the refractive index of biological components. Sensitivity S and figure of merit (FOM) are two important

indexes to measure the characteristics of sensors. For a refractive index sensor, the sensitivity *S* is defined as[51]:

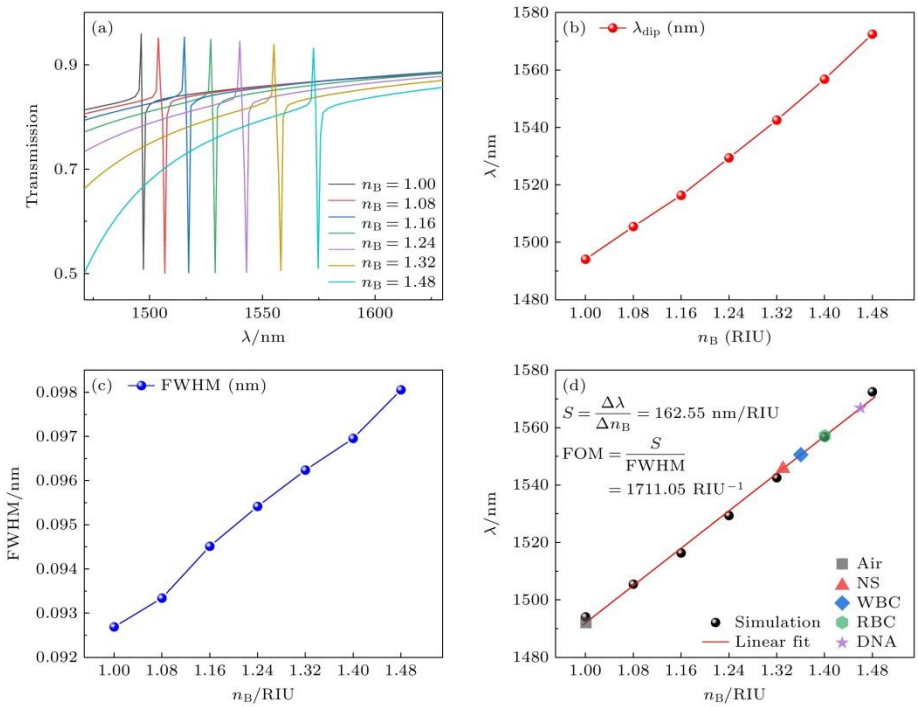

Figure 4. (a) Transmission spectra at different background refractive indices; (b) variation of resonance wavelength with background refractive index; (c) variation of half-height width FWHM with background refractive index; (d) linear fit to the variation of resonance wavelength with background refractive index redshift, the sensitivity *S* and the superior value FOM are calculated from the fitted gradient, the RIs of multiple biological components are labeled in the fitted straight line.

$$S = \frac{\Delta\lambda}{\Delta n_B}, \qquad (4)$$

Where Δ λ is the change in resonance wavelength position, Δn_B is the change in background refractive index, and the unit of *S* is nm/RIU. The figure of merit FOM is

$$\text{FOM} = S/\text{FWHM}, \qquad (5)$$

Where FWHM is the full width at half maximum of the resonance peak of the transmission spectrum, and the unit of FOM is RIU^{-1}. Corresponding to the data in the Fig. 4(b), the performance of the sensor is characterized by *S* = 165.22 nm/RIU, FOM = 1711.05 RIU at *r* = 25 nm^{-1}.

The Tab. 1 is the comparison of the sensing performance between the metasurface structure proposed in this paper and the structure proposed in the literature. It can be

seen that the structure designed in this paper has not only high sensitivity, but also high FOM and Q factor. At the same time, the designed metasurface as an optical platform in free space provides greater convenience for biosensing operation, and the simple structural design saves a lot of trouble for the actual etching preparation.

Table 1. Comparison of the sensing performance of different mechanisms of metasurface structures and the present study.

Mechanism	Materical	Q-factor	S/(nm·RIU^{-1})	FOM/RIU^{-1}	Reference
Surfaceplasmon	Au	121	250	28	[68]
Surfaceplasmon	Au	~40	450	28.8	[69]
Surfaceplasmon	Au	~8	170	1.3	[70]
SP-BIC	Si	3326	145	389	[71]
SP-BIC	Si	8428	160	575	[72]
SP-BIC	Si_3N_4	~10^3	178	445	[73]
Fano resonance	TiO2	5126	186.96	721	[74]
Accidental BIC	GaP	<10^4	135	<10^3	[39]
SP-BIC	Si	16506	162.55	1711.05	This work

4. Conclusion

In summary, a novel all-dielectric metasurface structure is proposed to realize refractive index sensing of biological proteins. The metasurface consists of periodically arranged silicon disks with eccentric holes on a glass substrate, which can support symmetry-protected bound States in a continuous medium. When the in-plane symmetry of the metasurface is broken, the SP-BIC is transformed into a QBIC with a high Q factor, thus realizing a Fano resonance with a sharp asymmetric line shape. The sensitivity of this resonance peak is very sensitive to the change of ambient refractive index, so it can be used for accurate sensing of biological refractive index. Based on the QBIC with high Q factor, this metasurface can achieve the sensitivity and figure of merit of 162.55 nm/RIU and 1711.05 RIU^{-1}, respectively, which are higher than many existing studies. Based on the high FOM sensing performance, the metasurface has lower ohmic loss and higher tunability than the traditional plasmonic metasurface. Therefore, this metasurface demonstrates significant application potential in cell scanning imaging and refractive index measurement of biological proteins, providing higher detection sensitivity and wider applicability.

References

[1] Sadreev A F 2021 *Rep. Prog. Phys.* **84** 055901

[2] Koshelev K, Bogdanov A, Kivshar Y 2019 *Sci. Bull.* **64** 836

[3] Huang L J, Li G Q, Gurarslan A, Yu Y L, Kirste R, Guo W, Zhao J J, Collazo R, Sitar Z, Parsons G N, Kudenov M, Cao L Y 2016 *ACS Nano* **10** 7493

[4] Neumann J V, Wigner E P 1929 *Phys. Z* **30** 465

[5] Tong H, Liu S Y, Zhao M D, Fang K J 2020 *Nat. Commun.* **11** 5216

[6] Linton C M, McIver P 2007 *Wave Motion* **45** 16

[7] Marinica D C, Borisov A G, Shabanov S V 2008 *Phys. Rev. Lett.* **100** 183902

[8] Plotnik Y, Peleg O, Dreisow F, Heinrich M, Nolte S, Szameit A, Segev M 2011 *Phys. Rev. Lett.* **107** 183901

[9] Hsu C W, Zhen B, Lee J, Chua S L, Johnson S G, Joannopoulos J D, Soljačić M 2013 *Nature* **499** 188

[10] Monticone F, Alù A 2014 *Phys. Rev. Lett.* **112** 213903

[11] Gomis-Bresco J, Artigas D, Torner L 2017 *Nat. Photonics* **11** 232

[12] Kodigala A, Lepetit T, Gu Q, Bahari B, Fainman Y, Kanté B 2017 *Nature* **541** 196

[13] Doeleman H M, Monticone F, den Hollander W, Alù A, Koenderink A F 2018 *Nat. Photonics* **12** 397

[14] Li Z Y, Chang H N, Lai J M, Song F L, Yao Q F, Liu H Q, Ni H Q, Niu Z C, Zhang J 2023 *J. Semicond.* **44** 082901

[15] Salmanogli A 2023 *J. Semicond.* **44** 052901

[16] Bulgakov E N, Sadreev A F 2008 *Phys. Rev. B* **78** 075105

[17] Romano S, Zito G, Lara Y épez S N, Cabrini S, Penzo E, Coppola G, Rendina I, Mocellaark V 2019 *Opt. Express* **27** 18776

[18] Liu H G, Zhang X Y, Nan X Y, Zhao E G, Liu H T 2024 *Acta Phys. Sin.* **73** 047802

[19] Srivastava Y K, Ako R T, Gupta M, Bhaskaran M, Sriram S, Singh R 2019 *Appl. Phys. Lett.* **115** 151105

[20] Liu D J, Wu F, Yang R, Chen L, He X Y, Liu F 2021 *Opt. Lett.* **46** 4370

[21] Koshelev K, Favraud G, Bogdanov A, Kivshar Y, Fratalocchi A 2019 *Nanophotonics* **8** 725

[22] Lee J, Zhen B, Chua S L, Qiu W, Joannopoulos J D, Soljačić M, Shapira O 2012 *Phys. Rev. Lett.* **109** 067401

[23] Hsu C W, Zhen B, Stone A D, Joannopoulos J D, Soljačić M 2016 *Nat. Rev. Mater.* **1** 1

[24] Xu L, Zangeneh Kamali K Z, Huang L J, Rahmani M, Smirnov A,

Camacho-Morales R, Ma Y X, Zhang G Q, Woolley M, Neshev D, Miroshnichenko A E 2019 *Adv. Sci.* **6** 1802119

[25] Paddon P, Young J F 2000 *Phys. Rev. B* **61** 2090

[26] Bulgakov E N, Sadreev A F 2014 *Opt. Lett.* **39** 5212

[27] Barrow M, Phillips J 2020 *Opt. Lett.* **45** 4348

[28] Zong X Y, Li L X, Liu Y F 2021 *Opt. Lett.* **46** 6095

[29] Jain A, Moitra P, Koschny T, Valentine J, Soukoulis C M 2015 *Adv. Opt. Mater.* **3** 1431

[30] Wang Y H, Fan Y B, Zhang X D, Tang H J, Song Q H, Han J C, Xiao S M 2021 *ACS Nano* **15** 7386

[31] Chen Y, Zhao C, Zhang Y Z, Qiu C W 2020 *Nano Lett.* **20** 8696

[32] Koshelev K, Lepeshov S, Liu M, Bogdanov A, Kivshar Y 2018 *Phys. Rev. Lett.* **121** 193903

[33] Alipour A, Farmani A, Mir A 2018 *IEEE Sensors J.* **18** 7047

[34] Kong Y, Cao J J, Qian W C, Liu C, Wang S Y 2018 *IEEE Photonics J.* **10** 6804410

[35] Bezus E A, Bykov D A, Doskolovich L L 2018 *Photon. Res.* **6** 1084

[36] Zeng T Y, Liu G D, Wang L L, Lin Q 2021 *Opt. Express* **29** 40177

[37] Al-Ani I A M, As'Ham K, Huang L, Miroshnichenko A E, Hattori H T 2021 *Laser Photonics Rev.* **15** 2100240

[38] Xiang J, Chen J, Lan S, Miroshnichenko A E 2020 *Adv. Opt. Mater.* **8** 2000489

[39] Li Z T, Panmai M, Zhou L D, Li S L, Liu S M, Zeng J H, Lan S 2023 *Appl. Surf. Sci.* **620** 156779

[40] Chen C, Wang J 2020 *Analyst* **145** 1605

[41] Sharma S, Kumari R, Varshney S K, Lahiri B 2020 *Reviews in Physics* **5** 100044

[42] Wang Z, Tan C H, Peng M, Yu Y Y, Zhong F, Wang P, He T, Wang Y, Zhang Z H, Xie R Z, Wang F, He S J, Zhou P, Hu W D 2024 *Light. Sci. Appl.* **13** 277

[43] Roingeard P, Raynal P I, Eymieux S, Blanchard E 2019 *Rev. Med. Virol.* **29** e2019

[44] Caucheteur C, Villatoro J, Liu F, Loyez M, Guo T, Albert J 2022 *Adv. Opt. Photon.* **14** 1

[45] Polz L, Dutz F J, Maier R R J, Bartelt H, Roths J 2021 *Optics & Laser Technology* **134** 106650

[46] Valušis G, Lisauskas A, Yuan H, Knap W, Roskos H G 2021 *Sensors* **21** 4092

[47] Toropov N, Cabello G, Serrano M P, Gutha R R, Rafti M, Vollmer F 2021 *Light Sci. Appl.* **10** 42

[48] Azzouz A, Hejji L, Kim K H, Kukkar D, Souhail B, Bhardwaj N, Brown R J C,

Zhang W 2022 *Biosens. Bioelectron.* **197** 113767

[49] Li Q, Meng J P, Li Z 2022 *J. Mater. Chem. A* **10** 8107

[50] Wang J, Kühne J, Karamanos T, Rockstuhl C, Maier S A, Tittl A 2021 *Adv. Funct. Mater.* **31** 2104652

[51] Guo L H, Zhang Z X, Xie Q, Li W X, Xia F, Wang M, Feng H, You C L, Yun M J 2023 *Appl. Surf. Sci.* **615** 156408

[52] https://www.lumerical.com/tcad-products/fdtd/ for FDTD method.

[53] Johnson S G, Joannopoulos J D 2001 *Opt. Express* **8** 173

[54] Xu T, Wheeler M S, Nair S V, Ruda H E, Mojahedi M, Aitchison J S 2008 *Appl. Phys. Lett.* **93** 241105

[55] Zhen B, Hsu C W, Lu L, Stone A D, Soljačić M 2014 *Phys. Rev. Lett.* **113** 257401

[56] Limonov M F, Rybin M V, Poddubny A N, Kivshar Y S 2017 *Nat. Photonics* **11** 543

[57] Miroshnichenko A E, Flach S, Kivshar Y S 2010 *Rev. Mod. Phys.* **82** 2257

[58] Yang Z J, Hao Z H, Lin H Q, Wang Q Q 2014 *Nanoscale* **6** 4985

[59] Hinamoto T, Fujii M 2021 *OSA Continuum.* **4** 1640

[60] Alaee R, Rockstuhl C, Fernandez-Corbaton I 2018 *Opt. Commun.* **407** 17

[61] Wang X, Duan J, Chen W, Zhou C, Liu T, Xiao S 2020 *Phys. Rev. B* **102** 155432

[62] Li Z, Xie M, Nie G, Wang J, Huang L 2023 *J. Phys. Chem. Lett.* **14** 10762

[63] Hu H, Lu W, Antonov A, Bertéa R, Maier S A, Tittl A 2024 *Nat. Commun.* **15** 7050

[64] Zhou C B, Liu G Q, Ban G X, Li S Y, Huang Q Z, Xia J S, Wang Y, Zhan M S 2018 *Appl. Phys. Lett.* **112** 101904

[65] Maji P S, Shukla M K, Das R 2018 *Sensor. Actuat. B: Chem.* **255** 729

[66] Bankapur A, Zachariah E, Chidangil S, Valiathan M, Mathur D 2010 *PLOS ONE* **5** e10427

[67] Tuchin V V, Zhestkov D M, Bashkatov A N, Genina E A 2004 *Opt. Express, OE* **12** 2966

[68] Chen J, Yuan J, Zhang Q, Ge H M, Tang C J, Liu Y, Guo B N 2018 *Opt. Mater. Express* **8** 342

[69] Gao B W, Wang Y L, Zhang T Z, Xu Y, He A X, Dai L, Zhang J S 2019 *ACS Nano* **13** 9131

[70] Sun F, Yang W C, Du C L, Chen Y X, Fu T Y, Shi D N 2020 *Plasmonics* **15** 949

[71] Li H, Yu S L, Yang L, Zhao T G 2021 *Optics Laser Technology* **140** 107072

[72] Song S, Yu S L, Li H, Zhao T G 2022 *Laser Phys.* **32** 025403

[73] Zito G, Sanità G, Alulema B G, Yépez S N L, Lanzio V, Riminucci F, Cabrini S, Moccia M, Avitabile C, Lamberti A, Mocella V, Rendina I, Romano S 2021

Nanophotonics **10** 4279

[74] Liu H G, Zheng L, Ma P Z, Zhong Y, Liu B, Chen X Z, Liu H T 2019 *Opt. Express* **27** 13252